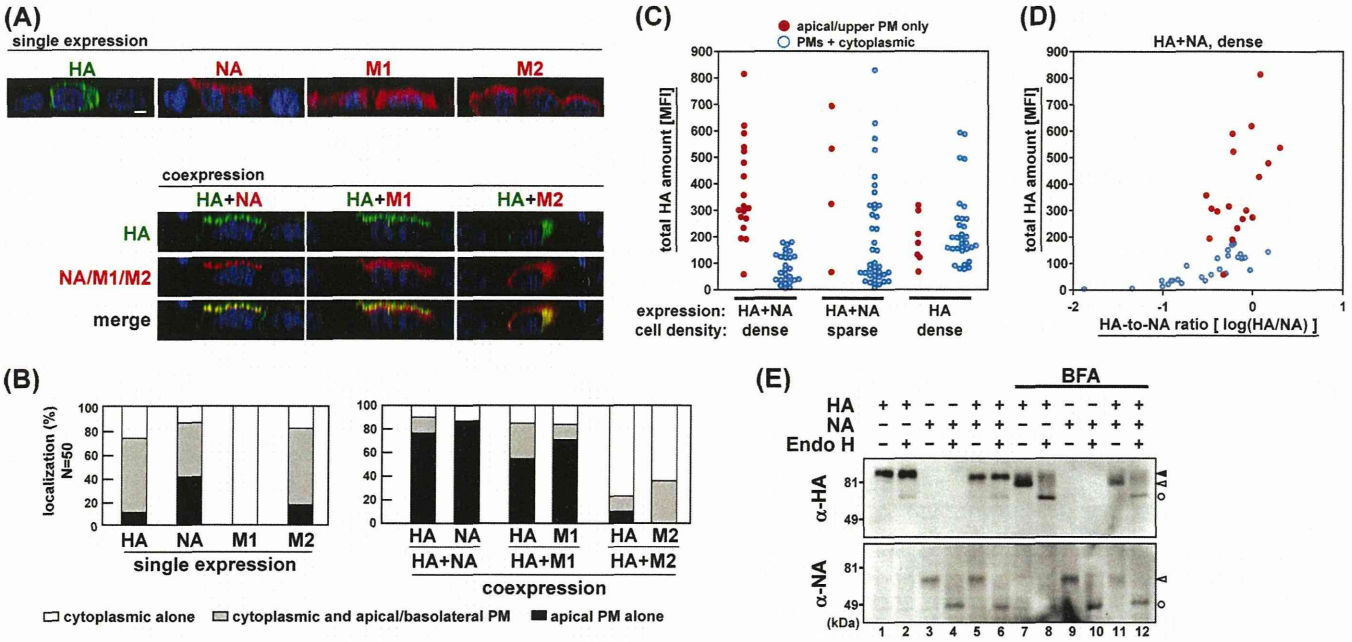

FIG 3 Acceleration of apical PM targeting of HA by coexpression with NA or M1. (A) Polarized MDCK cells were cotransfected with the combination of an HA expression plasmid and an NA, M1, or M2 expression plasmid. At 12 hpt, the cells were fixed and stained with anti-HA mAb12-1G6 (green) and sheep anti-NA, rabbit anti-M1, or mouse anti-M2 Ab (red). For costaining, anti-HA mAb12-1G6 and mouse anti-M2 Ab were prelabeled with Alexa Fluor dyes. Nuclei were stained with TO-PRO-3 (blue). Images in the *x-z* planes are shown. All images were taken at the same magnification. Scale bar, 10 μm. (B) In each experiment, 50 antigen-positive cells were subjected to analysis of the viral antigen distribution pattern. In coexpression experiments, 50 antigen double-positive (HA-positive and NA, M1, or M2-positive) cells were chosen and subjected to distribution pattern analysis for each viral protein. (C) Polarized MDCK cells (1×10^6 cells/well) or sparse MDCK cells (1×10^5 cells/well) were singly transfected with an HA or doubly transfected with HA and NA expression plasmids. At 12 hpt, intracellular viral antigens were stained with anti-HA mAb12-1G6 and rabbit anti-NA Ab. Nuclei were stained with DAPI. In each cell, the fluorescence intensities of serial confocal images were accumulated in *z* direction, and the MFIs were calculated. For HA localization, 39 or 45 HA-positive cells were analyzed and sorted into two categories (either apical PM alone or PMs plus cytoplasmic compartments). (D) The data of coexpression in polarized cells were also sorted by the ratio of the MFI of HA to NA. (E) Polarized MDCK cells were transfected with HA and/or NA expression plasmids. At 12 hpt, cells were harvested, and protein samples were treated with Endo H and analyzed by Western blotting with rabbit anti-HA and sheep anti-NA Abs. ▲, Endo H-resistant (complex glycan) forms; △, Endo H-sensitive (high mannose) forms; ○, Endo H-digested products. Brefeldin A (BFA) was added to the cells as an inhibitor of the transport of the protein from the endoplasmic reticulum to the Golgi compartment.

PM via transcytosis (30). Overall, these data indicated that the HA in infected cells was accumulated at the apical PM within another 4 or 5 h after the appearance of HA in the cytoplasmic compartments, such as the TGN.

To examine whether singly expressed HA followed similar transport kinetics, polarized MDCK cells were transfected with a plasmid expressing wt-HA and were subjected to immunofluorescence assays. The majority of HA was localized at the TGN at 9 hpt (84% of HA-positive cells), similar to the HA distribution pattern in infected cells at 4 hpi. Surprisingly, HA was broadly distributed in the cytoplasmic compartments even at 12 hpt. HA accumulation at the apical PM was observed in some cells at 24 hpt (40% of HA-positive cells) and became prominent at 48 hpt (Fig. 2A and C), suggesting that the apical targeting of HA in singly transfected cells was very slow compared with that of HA in infected cells.

Apical targeting of transfected HA was accelerated by superinfection. To investigate whether efficient apical targeting of HA required coexpression of viral components other than HA, polarized MDCK cells were transfected with the wt-HA expression plasmid, and, at 6 hpt, the cells were superinfected with the authentic PR8 virus, the HA of which was not reactive with mAb12-1G6. Immunostaining revealed that upon superinfection, the transfected HA became accumulated at the apical PM at 12 hpt (50% of HA-positive cells) (Fig. 2B and C). In contrast, transfected HA without superinfection was still localized in the cytoplasmic compartments (Fig. 2A and C). These data suggested that the apical PM targeting of HA was accelerated by the presence of other viral components.

Apical targeting of HA was accelerated by coexpression with NA or M1. Integral membrane proteins of influenza virus (HA, NA, and M2) are transported to the apical PM via the secretory pathway (31, 32, 33). Previous studies identified the apical sorting signal in the TMD of HA and NA (2, 3). M1 lacks an intrinsic apical sorting signal but has been suggested to be transported to the apical PM through association with HA, NA, and M2 CTs (7, 20). To identify the viral components responsible for the acceleration of apical targeting of HA, polarized MDCK cells were cotransfected with a combination of the HA expression plasmid and an NA, M1, or M2 expression plasmid. The cells were fixed at 12 hpt and were subjected to immunostaining with the anti-HA mAb12-1G6 and sheep anti-NA, anti-M1, or anti-M2 Ab (Fig. 3A). In singly transfected cells, a relatively large fraction of NA was accumulated at the apical PM at 12 hpt (40% of NA-positive cells). M1 was diffusely distributed in the cytoplasm and the nucleus, consistent with previous studies (34). M2 was observed both in the cytoplasmic compartments and at the apical/basolateral PMs. In doubly transfected cells, we found that HA was more accumulated at the apical PM when it was coexpressed with NA or M1 (79% in

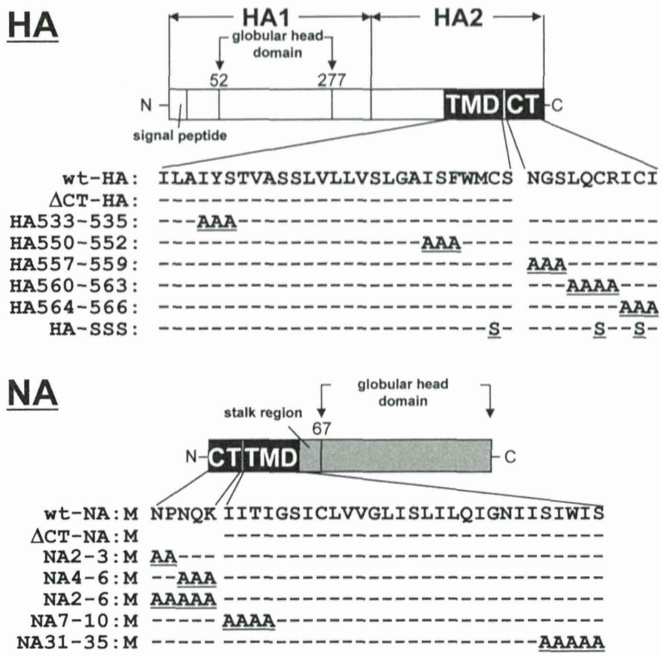

FIG 4 Schematic representation of HA and NA mutants. HA consists of the N-terminal HA1 and C-terminal HA2 subunits, the latter of which contains the TMD (27 amino acids) and CT (10 amino acids). NA consists of the N-terminal CT (5 amino acids) and TMD (29 amino acids), the stalk region, and the C-terminal globular head domain. Deletions are shown as blanks, and alanine or serine substitutions are underlined. Dashed lines indicate an absence of amino acid substitutions.

HA and NA double-positive cells; 52% in HA and M1 double-positive cells), suggesting that apical targeting of HA was accelerated by coexpression with NA or M1. Interestingly, apical targeting of NA and M1 was also accelerated by coexpression with HA, compared with the level in the singly transfected cells (85% versus 40% in the case of NA; 73% versus 0% in the case of M1) (Fig. 3A and B), suggesting that coexpression of HA with NA and M1 mutually accelerated their apical PM targeting.

In contrast, when HA was coexpressed with M2, apical targeting of HA and M2 was rather inhibited (Fig. 3A and B). The inhibition was also observed at a later time point (48 hpt) (data not shown). In cells expressing HA alone, HA was accumulated at the apical PM. In contrast, HA was distributed in the cytoplasmic compartments when M2 was coexpressed, suggesting that HA and M2 mutually interfered with their apical transport. This observation is in accordance with a previous study in which M2 inhibited the TGN release of apical secreted proteins (35). However, such inhibition was not apparent in infected cells. At 9 hpi, both HA and M2 accumulated at the apical PM (data not shown), suggesting that such inhibition may have been cancelled in the infected cells.

It is possible that high-level expression of HA and NA facilitates their apical targeting. To explore this possibility, intracellular expression levels of HA and NA were measured. In each cell, serial confocal *z* sections were collected at 0.5-μm intervals, and the MFI was calculated by summing the *z* stack. The MFIs were evaluated as total expression levels of HA and NA, and the cells were subjected to analysis of HA distribution patterns (either apical PM alone or PMs plus cytoplasmic compartments) (Fig. 3C). In singly transfected cells, apical accumulation of HA was not linked with the expression level of HA. In some cells, apical accumulation of HA was not seen even when the expression level of HA was high. In coexpressed cells, apical accumulation of HA was observed at various levels of HA expression (Fig. 3C) although the apical targeting was rarely seen at a very low level of HA expression (below the threshold of visible fluorescence intensity). These data suggested that the expression level of HA was not fully responsible for the apical targeting of HA. When the expression ratio of HA-to-NA was calculated from the total fluorescence intensities of HA and NA, no apparent relationship between the apical targeting of HA and the expression ratio of HA to NA was observed (Fig. 3D).

The endoplasmic reticulum-to-Golgi compartment transport is responsible for the apical protein trafficking. We employed Endo H digestion assays to explore whether HA coexpressed with NA was transported to the Golgi compartment faster than HA expressed alone. Results indicated that the sensitivity of HA to Endo H in the coexpressed cells was very similar to that of HA in singly expressed cells (Fig. 3E), suggesting that the acceleration of apical targeting of HA occurred at or after the Golgi compartment. The sensitivity of NA to Endo H in the coexpressed cells was also similar to that of NA in singly expressed cells (Fig. 3E) although the fact that a large fraction of NA seemed to be Endo H sensitive in Western blotting suggested that antibody-based detection in two different assays may not have detected the identical population of NA.

Mutations of HA/NA involved in the association with lipid rafts abrogated acceleration of their apical targeting. HA and NA are intrinsically associated with lipid raft microdomains, whereas M2 is excluded from these domains (5, 6). HA is a type I transmembrane (TM) protein and contains the regions responsible for lipid raft association in the CT and TMD (5, 7). Previous studies have shown that hydrophobic amino acids in the outer leaflet of the TMD (4, 5) and palmitoylation at three cysteine residues in the TMD-CT (8) are required for the association of HA with lipid rafts. One study has shown that deletion of the CT in HA reduces the lipid raft association without affecting the apical transport (7). NA is a type II TM protein, and the residues located at the TMD and CT are also involved in the association of NA with lipid rafts (3, 7).

To examine whether the lipid raft association of HA and NA was linked to the acceleration of their apical transport, we constructed HA and NA mutants with CT deletions (ΔCT-HA and ΔCT-NA) (Fig. 4). Polarized MDCK cells were cotransfected with a combination of these constructs and subjected to confocal microscopy at 12 hpt (Fig. 5A). In the singly transfected cells, ΔCT-HA was predominantly observed in the cytoplasmic compartments, and only 15% of HA-positive cells showed HA accumulation at the apical PM. This distribution pattern was similar to the localization pattern of wt-HA. ΔCT-NA was also localized mostly to the cytoplasmic compartments, suggesting less efficient apical transport than for the wt-NA (17% versus 30% of NA-positive cells) (Fig. 5A and C). When polarized MDCK cells were cotransfected with a combination of the wt-HA plus wt-NA, wt-HA plus ΔCT-NA, ΔCT-HA plus wt-NA, or ΔCT-HA plus ΔCT-NA constructs, we found that apical targeting of ΔCT-HA was not accelerated despite the coexpression with wt-NA (apical accumulation in 6% of ΔCT-HA and wt-NA double-positive cells), and, similarly, that apical targeting of ΔCT-NA was not accelerated despite the coexpression of wt-HA (apical accumula-

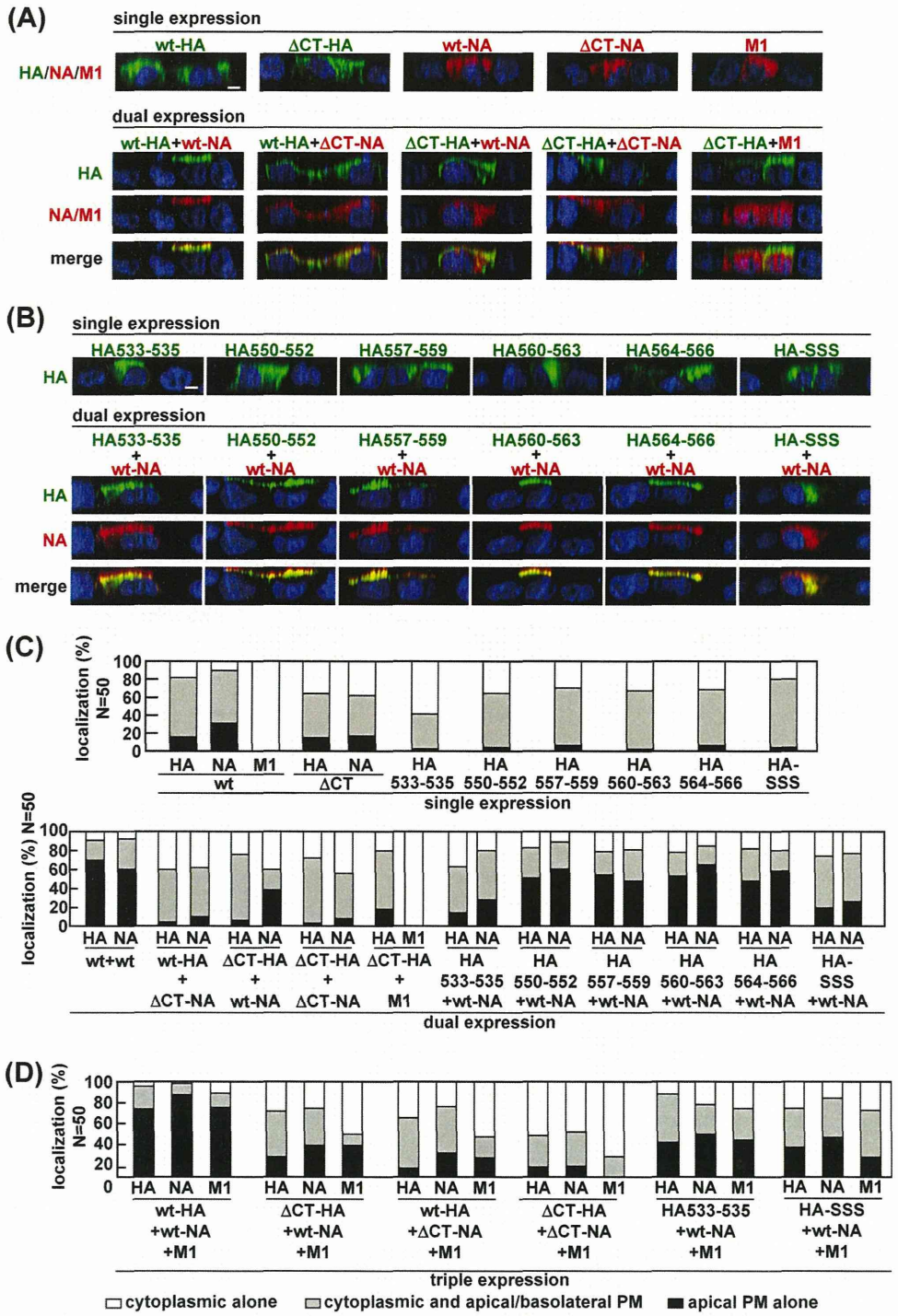

FIG 5 Apical PM targeting of HA and NA mutants with CT deletions and HA TMD mutants. Polarized MDCK cells were cotransfected with double (A and B) and triple (D) combinations of wt and HA and NA mutant expression plasmids, as indicated above the panels. At 12 hpt, the cells were stained with anti-HA mAb12-1G6 (green) and sheep anti-NA or anti-M1 Ab (red). Nuclei were stained with TO-PRO-3 (blue). All images were taken at the same magnification, and images in the *x-z* planes are shown. Scale bar, 10 μm. For semiquantification, 50 HA and NA or M1 double-positive cells (C) and 50 HA, NA, and M1 triple-positive cells (D) were subjected to antigen distribution pattern analysis, and the distribution patterns of each of HA, NA, and M1 were analyzed separately.

tion in 10% of wt-HA and ΔCT-NA double-positive cells) (Fig. 5A and C). These results suggested that both CT domains were necessary for the mutual acceleration of apical targeting of HA and NA. Several studies have shown that M1 is intrinsically not associated with the membrane but is targeted to the apical PM through the interaction with the CT domains of HA and NA (7, 20). Consistent with these reports, when M1 was coexpressed with ΔCT-HA, M1 failed to target the apical PM (compare Fig. 3 and 5).

Previous studies have shown that the amino acid sequences of the HA and NA TMDs spanning the outer leaflet of the lipid bi-

layer were critical for association with lipid rafts, whereas the sequences spanning the inner leaflet were less important (3, 5). We carried out alanine or serine substitution in the TMD-CT of HA (HA533–535, HA550–552, HA557–559, HA560–563, HA564–566, and HA-SSS) and NA (NA2–3, NA4–6, NA2–6, NA7–10, and NA31–35) (Fig. 4). The lipid rafts are defined as the membranes insoluble to nonionic detergent at 4°C (15, 36). We expressed these mutants in 293T cells and solubilized the membrane in the presence of 1% TX-100 at 4°C. TX-100 solubilization analysis showed that the ΔCT-HA, HA533–535, HA-SSS (with mutations at the three palmitoylation sites) (Fig. 6A, lanes 4, 6, and 16), ΔCT-NA, NA2–6, and NA31–35 (Fig. 6B, lanes 4, 10, and 14) were mainly distributed to the detergent-soluble fractions, suggesting the lack of lipid raft association. Next, they were expressed in polarized MDCK cells, and at 12 hpt the antigen localizations were analyzed by confocal microscopy (Fig. 5). In singly transfected cells, none of the HA mutants was accumulated at the apical PM, which was similar to the distribution pattern for the wt-HA (percentages of the respective cell populations are 2% for HA533–535, 4% for HA550–552, 6% for HA557–559, 2% for HA560–563, 6% for HA564–566, and 4% for HA-SSS) (Fig. 5A and C). When the HA mutants were coexpressed with wt-NA, apical targeting of HA550–552, HA557–559, 560–563, and HA564–566 was accelerated (51%, 54%, 53%, and 48% in HA and NA double-positive cells, respectively) (Fig. 5B and C). It should be noted that in these combinations, apical targeting of wt-NA also appeared to be accelerated. In contrast, apical targeting of HA533–535 (with mutations of the amino acids spanning the outer leaflet of the lipid bilayer) and HA-SSS was not accelerated, despite the coexpression of wt-NA (Fig. 5B and C).

We similarly investigated apical transport of the NA mutants. In singly transfected cells, apical targeting of NA2–6 and NA31–35 was slightly impaired (9% and 23% of NA-positive cells, respectively), compared with wt-NA, NA2–3, NA4–6, and NA7–10 (46%, 39%, 44%, and 42% of NA-positive cells, respectively) (Fig. 7A and C). When wt-HA was coexpressed with these NA mutants, the apical transport of wt-HA was accelerated by coexpression of NA2–3, NA4–6, and NA7–10 (50%, 55%, and 56% in HA and NA double-positive cells, respectively) but not by coexpression of NA2–6 or NA31–35 (11% and 25%, respectively) (Fig. 7A and C), suggesting that the entire CT and the region spanning the outer leaflet of the lipid bilayer in NA were important for acceleration of the apical transport of HA as well as NA. Since some studies have indicated that the association of HA with lipid rafts is dispensable for its apical targeting (5, 7), we examined the intracellular localization of the HA/NA mutants that failed to target to the apical PM (e.g., ΔCT-HA, HA533–535, HA-SSS, ΔCT-NA, NA2–6, and NA31–35) at later time points. As expected, even in the singly transfected cells, these HA/NA mutants were accumulated at the apical PM in more than 70% of HA- or NA-positive cells at 48 hpt, indicating that their apical transport was not blocked but was slowed (data not shown).

Our data suggested that the acceleration of apical targeting of HA and NA was linked with their lipid raft associations. To confirm this, MDCK cells coexpressing wt-HA and wt-NA were treated with MβCD and lovastatin for depletion of cholesterol and were similarly analyzed by confocal microscopy. As expected, HA and NA were poorly accumulated at the PM (8% and 16%, respectively) (Fig. 7B and C).

We also tested whether these defective mutants were targeted

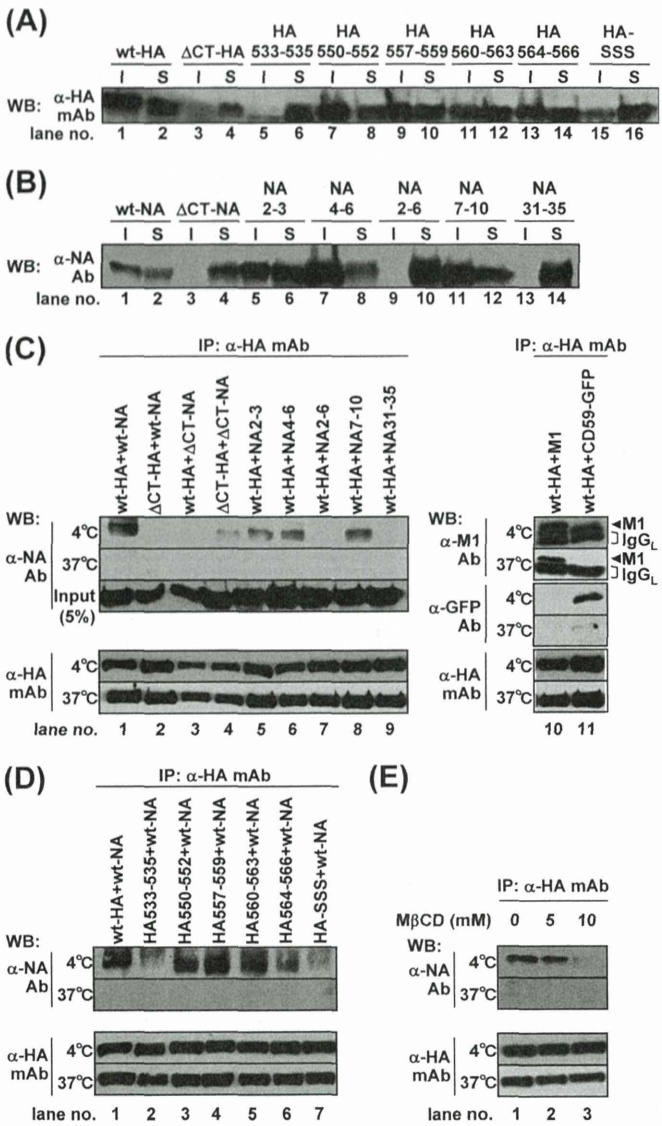

FIG 6 TX-100 solubility of HA and NA and interaction of HA and NA through lipid rafts. For the TX-100 solubilization test, 293T cells were singly transfected with mutant HA (A) or NA (B) expression plasmids (indicated). The cells were lysed with TNE buffer containing 1% TX-100 at 4°C for 30 min. Insoluble (I) and soluble (S) fractions were separated by centrifugation. For the interaction of HA and NA, cells were cotransfected with wt-HA and mutant NA expression plasmids (indicated) (C) or with mutant HA and wt-NA expression plasmids (indicated) (D). M1 was used as a positive control for direct interaction with HA, and GFP-CD59 was used as a marker for lipid rafts. The cells were lysed with TNE buffer containing 1% TX-100 at 4°C or 37°C for 30 min and were subjected to coimmunoprecipitation with anti-HA mAb12-1G6. Precipitates were analyzed by Western blotting using sheep anti-NA, anti-M1, and anti-GFP Abs and anti-HA mAb12-1G6. (E) For the cholesterol depletion experiment, 293T cells were pretreated with lovastatin for 12 h, cotransfected with wt-HA and wt-NA expression plasmids, and incubated at 37°C in the presence of lovastatin. At 24 hpt, the cells were further treated with lovastatin plus 5 mM or 10 mM MβCD for 1 h and were subjected to coimmunoprecipitation experiments. WB, Western blotting; mAb, mAb12-1G6; IP, immunoprecipitation.

to the apical PM when they were triply expressed with their wt-HA/NA counterparts plus additional M1 (Fig. 5D and 7D). In the cells triply transfected with wt-HA, wt-NA, and M1, apical targeting of wt-HA and wt-NA was accelerated at a level similar to that

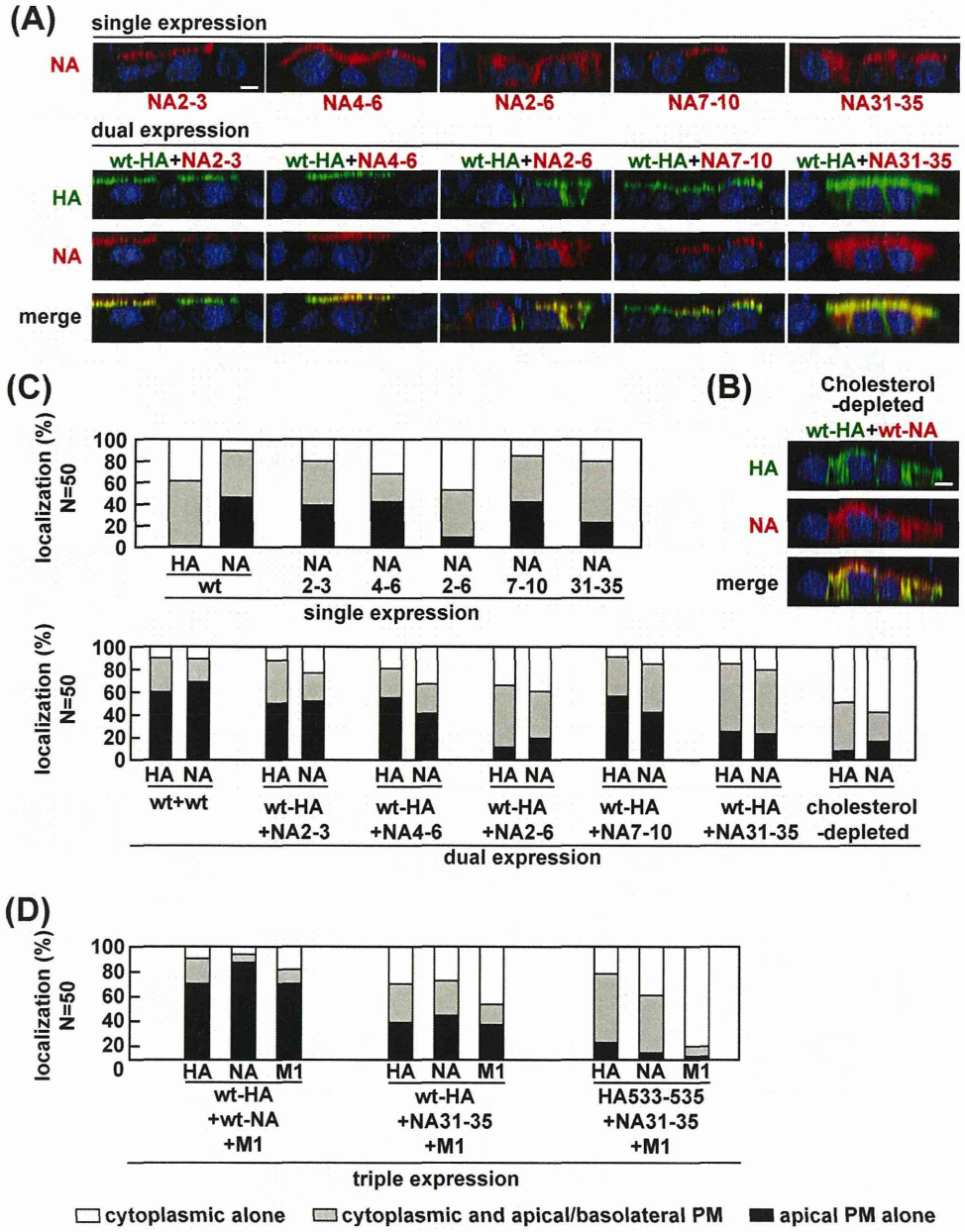

FIG 7 Apical PM targeting of NA TMD mutants and the effect of cholesterol depletion. Polarized MDCK cells were cotransfected with double (A) and triple (D) combinations of wt HA and NA and mutant expression plasmids, as indicated above the panels. (B) For the cholesterol depletion experiment, polarized MDCK cells were pretreated with lovastatin for 12 h and then cotransfected with wt-HA and wt-NA expression plasmids. After 11 h of incubation at 37°C with lovastatin, the cells were further treated with MβCD for 1 h at 37°C. At 12 hpt, the cells were stained with anti-HA mAb12-1G6 (green) and sheep anti-NA Ab (red). Nuclei were stained with TO-PRO-3 (blue). All images were taken at the same magnification, and images in the *x-z* planes are shown. Scale bar, 10 μm. For semiquantification, 50 HA and NA double-positive cells (C) and 50 HA, NA, and M1 triple-positive cells (D) were subjected to distribution pattern analysis as described in the legend of Fig. 5.

in cells with dual expression of wt-HA and wt-NA, indicating that M1 had no additive effect on the apical targeting of wt-HA and wt-NA (Fig. 5D and 7D). Similarly, when either HA or NA contained CT deletions, their apical targeting was hardly accelerated by coexpression with additional M1. This was most likely due to the lack of M1 binding sites within the CTs of HA and NA. Only slight acceleration of apical targeting was observed when HA533–535, NA31–35, or HA-SSS was coexpressed with its wt-HA/NA counterpart plus M1 (Fig. 5D and 7D). These results indicated that M1 did not sufficiently rescue the apical targeting defects of the HA and NA mutants.

Interaction of HA with NA via lipid rafts was required for acceleration of their apical targeting. To analyze the association of HA and NA via lipid rafts, the HA and NA mutants were coexpressed in 293T cells and were subjected to coimmunoprecipitation using anti-HA mAb12-1G6 (Fig. 6C and D). We first coexpressed the wt-HA and GFP-CD59 (a lipid raft marker) and solubilized the membrane with 1% TX-100. GFP-CD59 was co-

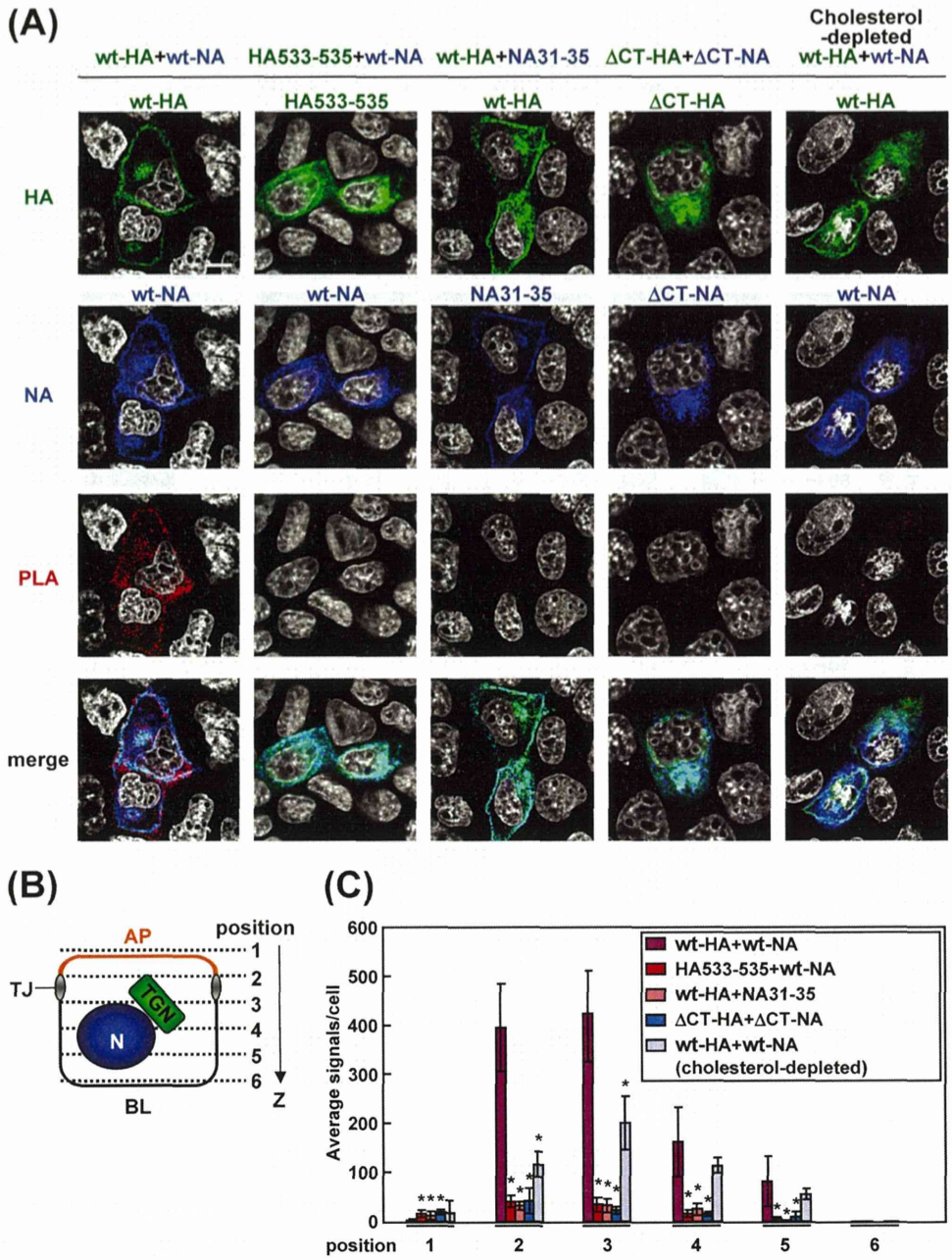

FIG 8 Accumulation of nonraft HA and NA mutants in transfected cells. (A) Polarized MDCK cells were cotransfected with expression plasmids for a combination of wt-HA plus wt-NA, HA533–535 plus wt-NA, wt-HA plus NA31–35, or ΔCT-HA plus ΔCT-NA. At 9 hpt, the cells were fixed, permeabilized, and incubated with two primary Abs (anti-HA mAb12-1G6 and rabbit anti-NA Ab). For PLA, the cells were incubated with anti-rabbit and anti-mouse proximity ligation secondary Abs conjugated with oligonucleotides (PLA probes). Following ligation of the probes and rolling-circle amplification, the rolling-circle products were detected by hybridization with their complementary oligonucleotides labeled with a fluorophore (excitation wavelength, 594 nm; emission wavelength, 624 nm) (red). The cells were further costained with anti-mouse Alexa Fluor 488 (for HA; green), anti-rabbit Alexa Fluor 647 (for NA; blue), and DAPI (gray). Scale bar, 10 μm. (B) A schematic diagram of six confocal *z* slices (positions 1 to 6) from the apical (AP) to basolateral (BL) side of the cell is shown. TJ, tight junction; N, nucleus. (C) The PLA signals at positions 1 to 6 were automatically counted using BlobFinder software, and the average number of signals in each *x-y* plane is shown. In each plane, the numbers in the coexpression samples (indicated) were compared with the number in the sample coexpressed with wt-HA and wt-NA. Asterisks represent statistically significant differences ($P < 0.05$) by Student's *t* test. The details of the cholesterol depletion experiment are described in the legend of Fig. 6B.

immunoprecipitated with wt-HA at 4°C but not at 37°C, indicating that both CD59 and wt-HA were associated with lipid rafts (Fig. 6C, lane 11). We used M1 as a positive control in the coimmunoprecipitation assays because M1 has been shown to interact directly with HA (7). We found that M1 was coimmunoprecipitated with wt-HA even when the lipid rafts were disrupted by TX-100 at 37°C (Fig. 6C, lane 10). When wt-HA was coexpressed with wt-NA or mutant NAs, some NA mutants (e.g., NA2–3, NA4–6, and NA7–10) were coimmunoprecipitated with wt-HA at 4°C although the efficiencies varied (Fig. 6C, lanes 1, 5, 6, and 8).

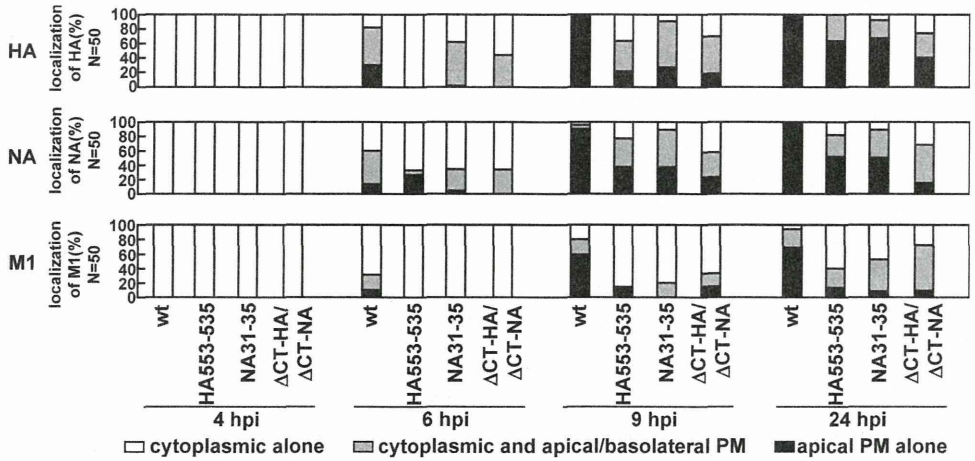

FIG 9 Temporal study of apical PM targeting of HA, NA, and M1 in cells infected with nonraft mutant viruses. Polarized MDCK cells were infected with the wt or nonraft mutant (HA533–535, NA31–35, or ΔCT-HA/ΔCT-NA) virus. At various time points, the cells were costained with anti-HA mAb12-1G6, sheep anti-NA, and anti-M1 Abs. The localizations of HA, NA, and M1 were analyzed in the *x-z* planes. For semiquantification of HA, NA, and M1 localization, 50 antigen-positive cells were chosen in each experiment, and the distribution patterns of each viral protein were counted separately.

In contrast, wt-HA failed to coprecipitate ΔCT-NA, NA2–6, and NA31–35 at 4°C, all of which were incapable of accelerating the apical targeting of wt-HA (Fig. 6C, lanes 3, 7, and 9). Conversely, when wt-NA was coexpressed with HA mutants and was similarly subjected to immunoprecipitation analysis, we found that HA550–552, HA557–559, HA560–563, and HA564–566 coprecipitated wt-NA at 4°C (Fig. 6D, lanes 3, 4, 5, and 6). In contrast, ΔCT-HA, HA533–535, and HA-SSS, all of which failed to accelerate the apical transport of wt-NA, coprecipitated wt-NA inefficiently (Fig. 6C, lane 2, and D, lanes 2 and 7). In all combinations, NA was not coimmunoprecipitated with HA when the lipid rafts were solubilized by treatment with TX-100 at 37°C. Thus, we depleted cholesterol from the cells by treatment with MβCD and lovastatin to disrupt the lipid rafts. wt-NA was not coimmunoprecipitated with wt-HA when the cells were treated with 10 mM MβCD (Fig. 6E, lane 3). Taken together, these data indicated that the interaction of HA with NA via lipid rafts was linked to the acceleration of their apical transport.

Proximal accumulation of HA and NA in lipid rafts. It has been considered that the TGN and apical recycling endosome are sorting platforms to route proteins to their destinations (37, 38). Recent studies have suggested that protein oligomerization or clustering in lipid rafts plays a pivotal role for segregation of apical cargos from basolateral cargos at the TGN and generation of intracellular transport vesicles (17, 39, 40). To examine whether HA and NA were accumulated in close proximity in lipid rafts, we prepared transfected cells at 9 hpt, when the majority of antigens were localized at the TGN, and performed *in situ* PLA. This method uses two primary antibodies specific for two target proteins and two oligonucleotide-conjugated and species-specific secondary antibodies (PLA probes) and detects the two targets in close proximity (<40 nm). After the PLA reaction, the cells were costained with Alexa Fluor-conjugated secondary Abs. Many PLA signals were observed in the cells coexpressing wt-HA and wt-NA (Fig. 8A). Confocal images were taken at 6 *z* slices (position 1 to 6) from the apical to basolateral aspects (Fig. 8B). The PLA signals in each *x-y* plane were automatically counted with BlobFinder software (Fig. 8C). The majority of PLA signals produced by the combination of the wt-HA and wt-NA were present at *z* positions 2 and 3, corresponding to the location of the TGN (see Fig. 10B), and some signals were in the cytoplasm (Fig. 8B). In contrast, PLA signals were rarely seen when either HA or NA was defective in lipid raft association (e.g., ΔCT-HA, HA533–535, ΔCT-NA, or NA31–35) (Fig. 8A). The numbers of their PLA signals were reduced more than 10-fold, compared with that obtained by the combination of the wt-HA and wt-NA (Fig. 8C). No significant differences in the expression levels of HA and NA were observed between the wt and mutants (Fig. 8A). These data indicated that HA and NA came into very close proximity, most likely clustering in lipid rafts, when their TMDs and CTs were intact. To confirm this, cholesterol was depleted from the cells by treatment with MβCD and lovastatin. The PLA signals in cells coexpressed with wt-HA and wt-NA were dramatically decreased by the disruption of lipid rafts (Fig. 8A and C). These data suggested that the lipid rafts were platforms for cytoplasmic accumulation of HA and NA.

Apical transport and proximal accumulation of nonraft-associated HA/NA were also inefficient in infected cells. We generated a recombinant virus with a mutation in either the HA or NA TMD (HA533–535 or NA31–35) and a virus with deletion of both CTs (ΔCT-HA/ΔCT-NA) by means of a reverse genetic procedure. Polarized MDCK cells were infected with the wt, HA533–535, NA31–35, or ΔCT-HA/ΔCT-NA virus, and the localization of viral antigens was similarly analyzed by confocal microscopy at 4, 6, 9, and 24 hpi (Fig. 9). In the case of the wt virus, HA and NA were localized to the cytoplasmic compartments at 4 hpi (100% of infected cells). M1 was diffusely distributed throughout the cells. At 9 hpi, HA, NA, and M1 were accumulated at the apical PM (100%, 100%, and 69%). When cells were infected with the nonraft-associated mutant viruses (HA533–535, NA31–35, and ΔCT-HA/ΔCT-NA), apical PM targeting of the viral components was significantly delayed. For example, at 9 hpi, accumulation of HA, NA, and M1 at the apical PM was observed in much smaller numbers of cells (Fig. 9).

We examined the accumulation/clustering of HA and NA in cells infected with these mutant viruses by *in situ* PLA (Fig. 10). In the wt-infected cells, PLA signals partially colocalized with TGN46

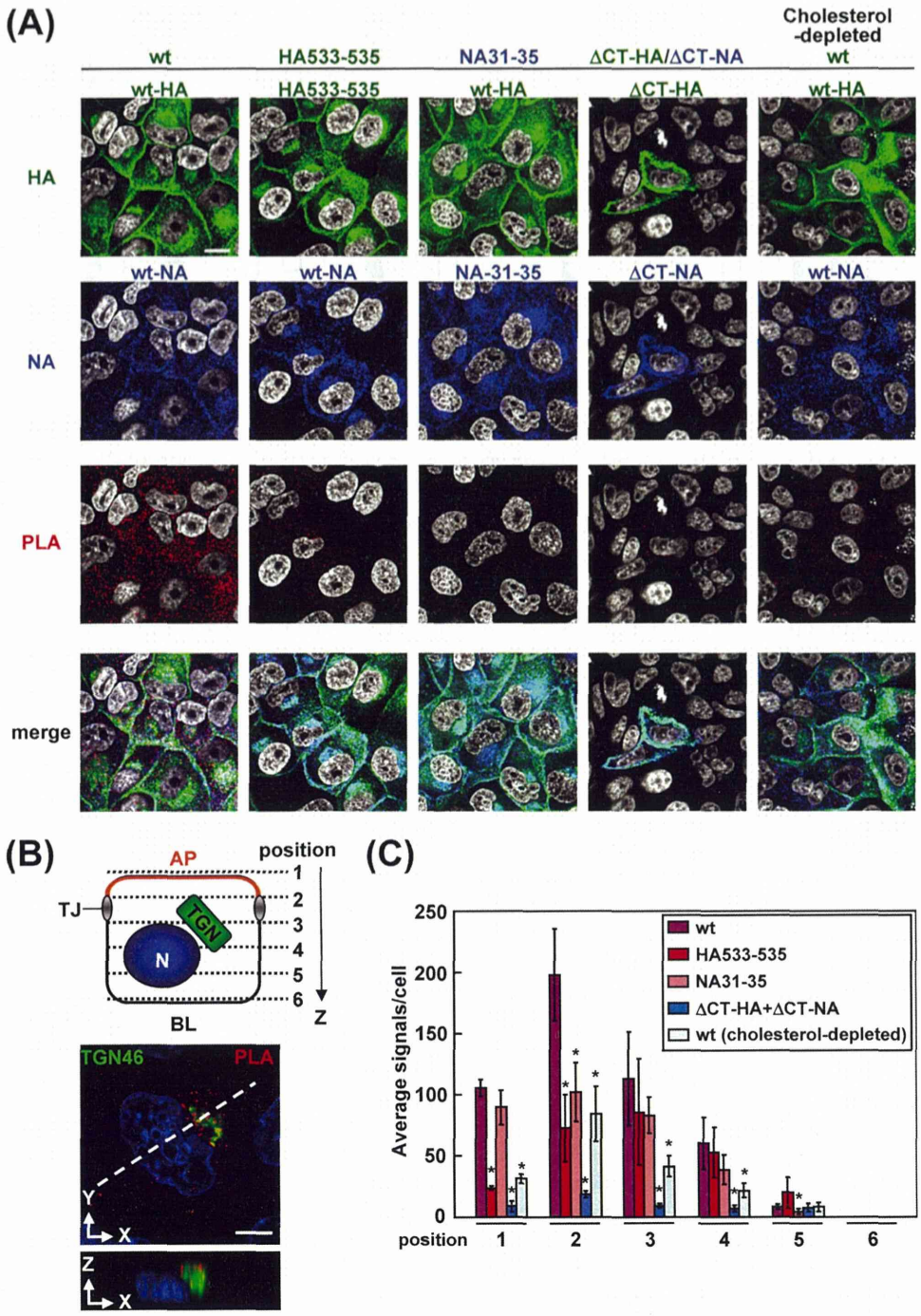

FIG 10 Accumulation of HA and NA in cells infected with nonraft mutant viruses. (A) Polarized MDCK cells were infected with the wt virus or HA533–535, NA31–35, or ΔCT-HA/ΔCT-NA mutant virus. At 5 hpi, the cells were fixed, permeabilized, and incubated with two primary Abs (anti-HA mAb12-1G6 and rabbit anti-NA Ab). PLA was carried out as described in the legend of Fig. 8A. Following PLA reaction, the cells were costained with anti-mouse Alexa Fluor 488 (for HA; green) and anti-rabbit Alexa Fluor 647 (for NA; blue). (B) A schematic diagram of six confocal *z* slices (positions 1 to 6) from the AP to the BL side of the cell is shown. MDCK cells were infected with the wt virus and subjected to PLA with two primary Abs (anti-HA mAb12-1G6 and rabbit anti-NA Ab) at 3.5 hpi. The cells were stained with prelabeled anti-TGN46 Ab. Localizations of the TGN46 (green) and PLA signals (red) are shown in the *x-y* and *x-z* planes. The dashed line in the *x-y* image indicates the positions of the *x-z* image. Scale bar, 10 μm. (C) The PLA signals at positions 1 to 6 were automatically counted using BlobFinder software. The average number of PLA signals in each *x-y* plane is shown in the graph. In each *x-y* plane, the numbers in the mutant virus samples (indicated) were compared with the number in the wt virus sample. Asterisks represent statistically significant differences ($P < 0.05$) by Student's *t* test.

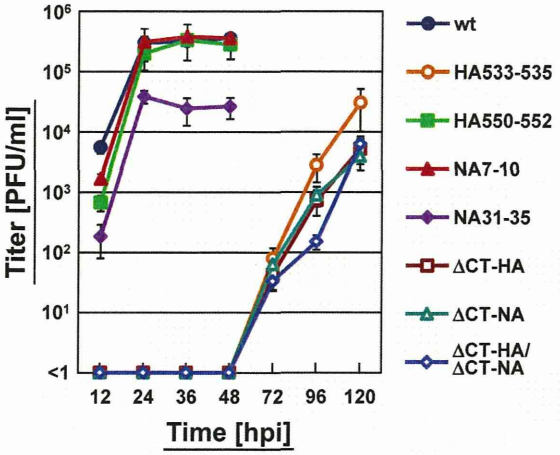

FIG 11 Growth kinetics of HA and NA mutant viruses. MDCK cells were infected with the wt or mutant virus at an MOI of 0.1. At various time points (12, 24, 36, 48, 72, 96, and 120 hpi), an aliquot of the culture medium was harvested, and virus titers were measured by plaque assay on MDCK cells.

were observed at 3.5 hpi (Fig. 10B), but no PLA signals were seen at 3 hpi. This result suggested that the lipid rafts functioned as platforms for cytoplasmic accumulation of HA and NA. Many PLA signals were observed broadly in the cytoplasm at 5 hpi (Fig. 10A and C). In contrast, PLA signals were rarely seen when the cells were infected with the HA533–535, NA31–35, or ΔCT-HA/ΔCT-NA virus. The numbers of their PLA signals were reduced more than 2-fold compared with that of the wt virus. Cholesterol depletion by the treatment with MβCD and lovastatin resulted in a similar reduction in the numbers of the PLA signals (Fig. 10A and C). These results were not ascribable to the protein expression levels (Fig. 10A). These data were consistent with the results of the coexpression experiments although the differences in the signal numbers were much more significant in the transfected cells (Fig. 8), suggesting that the lipid raft association of HA and NA in infected cells was still necessary for their efficient apical targeting and clustering.

Lipid raft association of HA and NA was required for efficient virus replication. We examined the growth kinetics of the mutant viruses by plaque assay (Fig. 11). Compared with the wt virus, the majority of the nonraft-associated mutant viruses (HA533–535, ΔCT-HA, ΔCT-NA, and ΔCT-HA/ΔCT-NA) grew significantly more slowly. A previous study has shown that nonraft-associated HA viruses do not grow for first 30 h and then grow slowly at low MOIs because of multiple defects: a budding defect and fusion defect (5). The nonraft-associated mutant virus NA31–35 had a titer 10-fold lower than the wt virus. It has been reported that the NA31–35 mutation results in a great reduction in sialidase activity and aggregation of virus particles on the infected cell surface (41). In contrast, raft-associated mutant viruses (HA550–552 and NA7–10) showed growth rates and titers similar to those of the wt virus (Fig. 11). Together, these data are consistent with previous studies in which recombinant viruses containing nonraft-associated HA and/or NA mutants had titers 10- to 1,000-fold lower than their parental virus (5, 42).

Coexpression of HA and NA facilitated apical targeting and clustering of cellular raft-associated proteins. Our data indicated that the coexpression of HA and NA facilitated their apical transport if they were raft associated. To examine whether the apical transport of cellular raft-associated proteins was affected upon coexpression of HA and NA, we carried out dual or triple expression experiments. CD59, a GPI-AP, is a well-known marker for lipid rafts and is transported to the apical PM. In singly transfected cells, the majority of CD59 was localized in the cytoplasmic compartments at 12 hpt (apical PM accumulation in 10% of CD59-positive cells). p75-GFP is also targeted to the apical PM but without lipid raft association (43). p75-GFP was similarly found in the cytoplasmic compartments at 12 hpt (apical accumulation in 5% of p75-GFP-positive cells). When CD59 was coexpressed with HA plus NA, apical targeting of CD59 was significantly accelerated (62% of CD59-positive cells), concomitant with the acceleration of apical targeting of HA/NA, indicating that coexpression of HA and NA similarly accelerated the apical transport of noncognate raft-associated proteins. In sharp contrast, apical targeting of p75-GFP was unaffected (apical targeting in 17% of p75-positive cells) when HA and NA were coexpressed even though apical targeting of HA and NA was accelerated (Fig. 12A). Such acceleration was not seen in coexpression with either HA or NA. These results indicated that coexpression of HA plus NA accelerated the apical targeting of raft-associated CD59 but not that of nonraft p75-GFP.

Recent studies have suggested that the clustering of raft-associated proteins may drive the coalescence of lipid rafts, leading to membrane curvature for vesicle budding (17, 39, 44, 45, 46). We investigated this possibility in cells coexpressing HA and NA. Caveolae are a subdomain of lipid raft microdomains (47, 48). We focused on two raft microdomains, caveolin-1-containing rafts and CD59-containing lipid rafts, and examined the coalescence of the two raft fractions by PLA. To this end, we carried out dual or triple expression experiments as before. The cells were fixed at 9 hpt when transfected antigens were present at the cytoplasmic compartments and were analyzed for the PLA signals between CD59 and endogenous caveolin-1. When CD59 was coexpressed with HA, some PLA signals were observed in the cytoplasm. When CD59 was coexpressed with HA plus NA, the PLA signals were significantly increased, indicating that upon coexpression of HA and NA, CD59 and caveolin-1, which were present in distinct raft fractions, came into close proximity. In contrast, when p75-GFP was coexpressed with HA plus NA, the number of PLA signals was lower than that in cells coexpressed with CD59 and HA (Fig. 12B). These findings were confirmed by quantification of the PLA signals in the *x-y* planes at six *z* positions (Fig. 12B). These results clearly indicated that coexpression of HA and NA also induced accumulation of lipid raft proteins, caveolin-1 and CD59, but not nonraft p75, suggesting the coalescence of membrane raft microdomains.

DISCUSSION

Coexpression of HA and NA induces lipid raft clustering, leading to efficient apical trafficking. The influenza virus HA has served as an apical marker in the research field of cell polarity and membrane trafficking (49, 50, 51). NA is also sorted to the apical PM (3, 14). Although the molecular mechanism of the apical transport of these envelope proteins has not been fully understood, previous studies have indicated that their TMD and CT possess determinants for the apical transport and lipid raft association (2, 3, 7). In this study, we found that in polarized cells the apical targeting of HA was accelerated when NA was coexpressed. This acceleration appeared to occur not before but after the Golgi

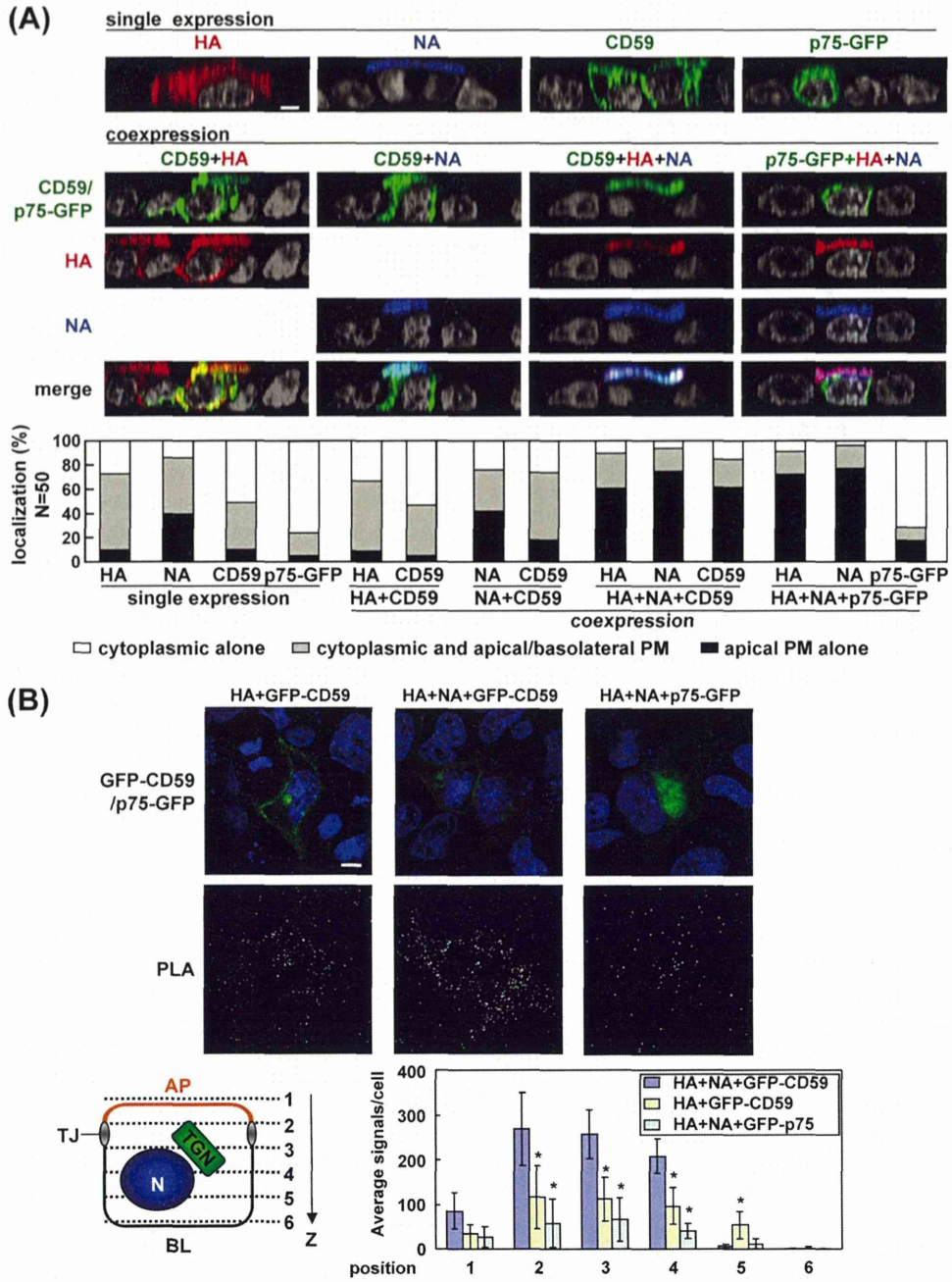

FIG 12 Apical targeting and clustering of raft and nonraft proteins by coexpression of HA and NA. (A) Polarized MDCK cells were cotransfected with a combination of wt-HA plus CD59 (apical and raft marker), wt-NA plus CD59, wt-HA and wt-NA plus CD59, or wt-HA and wt-NA plus p75-GFP (apical and nonraft marker) expression plasmids. For the immunofluorescence assay, cells were fixed at 12 hpt and stained with anti-CD59 (green) Ab, anti-HA mAb12-1G6 (red), and sheep anti-NA Ab (blue). Nuclei were stained with DAPI (gray). All images were taken at the same magnification, and images in the *x-z* plane are shown. (B) For PLA, the cells were fixed at 9 hpt, permeabilized, and incubated with two primary Abs (mouse anti-GFP Ab and rabbit anti-caveolin-1 Ab). PLA was performed as described in the legend of Fig. 8A. Scale bar, 10 μm. A schematic diagram of six confocal *z* slices (positions 1 to 6) from the AP to the BL side of the cell is shown. The PLA signals in the *x-y* planes at positions 1 to 6 were automatically counted using BlobFinder software, and the average number of signals in each *x-y* plane is shown. In each *x-y* plane, the numbers in the coexpression samples (indicated) were compared with the number in the sample coexpressed with wt-HA and wt-NA plus GFP-CD59. Asterisks represent statistically significant differences ($P < 0.05$) by Student's *t* test.

compartment (Fig. 3E), consistent with our findings that the acceleration was linked with the lipid raft association of HA and NA. It is known that lipid rafts are generated at the Golgi compartment in mammalian cells (15). Our quantitative analysis of HA/NA expression revealed that the apical targeting of HA was not linked with the expression level of HA (Fig. 3C). The analysis also indicated that the apical targeting of HA was inefficient without NA but that no certain molar ratio of HA to NA was observed for the acceleration of their apical targeting (Fig. 3D). Interestingly, in sparse, likely nonpolarized MDCK cells, the accumulation of HA